General Disclaimer

One or more of the Following Statements may affect this Document

- This document has been reproduced from the best copy furnished by the organizational source. It is being released in the interest of making available as much information as possible.

- This document may contain data, which exceeds the sheet parameters. It was furnished in this condition by the organizational source and is the best copy available.

- This document may contain tone-on-tone or color graphs, charts and/or pictures, which have been reproduced in black and white.

- This document is paginated as submitted by the original source.

- Portions of this document are not fully legible due to the historical nature of some of the material. However, it is the best reproduction available from the original submission.

X-552-70-409
PREPRINT

COMPARISON OF LUNAR GRAVITY FIELDS USING GSFC RANGE-RATE DATA FROM AIMP-E

VICTOR T. LACZO

NOVEMBER 1970

GSFC
GODDARD SPACE FLIGHT CENTER
GREENBELT, MARYLAND

X-552-70-409

COMPARISON OF LUNAR GRAVITY FIELDS USING GSFC RANGE-RATE DATA FROM AIMP-E

Victor T. Laczo
Mission Trajectory Determination Branch
Mission & Trajectory Analysis Division

November 1970

GODDARD SPACE FLIGHT CENTER
Greenbelt, Maryland

COMPARISON OF LUNAR GRAVITY FIELDS USING GSFC RANGE-RATE DATA FROM AIMP-E

Victor T. Laczo
Mission Trajectory Determination Branch
Mission & Trajectory Analysis Division

ABSTRACT

Two consecutive three-day arcs of unsmoothed VHF Doppler tracking data from the Goddard Range and Range Rate System (GRARR) were used to determine lunar orbits for AIMP-E (Explorer 35). This study yielded magnitudes for Doppler residuals and estimates for trajectory errors as a function of five lunar gravity models. To a certain extent this analysis permits evaluation of the GRARR System tracking a lunar orbiting satellite. An additional purpose of this report is to relate orbit prediction quality as a function of various lunar gravity models. The trajectory differences were best minimized by the Field 15 potential model which was derived from an analysis of orbital motion of Apollo 8.

CONTENTS

TABLES

COMPARISON OF LUNAR GRAVITY FIELDS USING GSFC RANGE-RATE DATA FROM AIMP-E

1. INTRODUCTION

The orbit of AIMP-E (launched on July 19, 1967) is markedly different from that of the other lunar satellites in the Apollo and Lunar Orbiter series. The orbit has a minimum height above the lunar surface of 790 kilometers with an eccentricity of 0.5739. Since AIMP-E has such a high orbit, lunar mass concentration effects are negligible and only the major terms in the lunar gravitational potential and the perturbations due to the sun and the earth effect the AIMP-E orbit.

The STADAN network is still tracking AIMP-E in lunar orbit using the VHF GRARR system. Some studies have been made to evaluate the lunar satellite tracking capability of the GRARR VHF system. Since future lunar orbiting satellites, such as Radio Astronomy Explorer (RAE-B), will also use VHF range-rate data, the following analysis also has a direct application.

There are two practical methods of estimating the lunar satellite tracking capability of Stadan VHF GRARR range-rate data. One method is to determine the magnitude of the Doppler frequency residuals in a converged solution for the AIMP-E orbit. Another approach is to determine the accuracy with which one can project or predict an orbit based on VHF Doppler observations. In this report trajectory evaluations were performed for each of five lunar potential models. The magnitudes of the position differences obtained in the various trajectory intercomparisons give an indication of the prediction capability of each gravity model.

2. AIMP-E ORBITAL SOLUTIONS

To study the orbit of AIMP-E, two consecutive three-day data arcs of VHF two-way Doppler data were obtained. The data were obtained by tracking stations operating at an uplink frequency of 148.26 MHz and a downlink frequency of 12/13 the uplink frequency. The summary of contents for each data arc is listed in Table 1. Included in this table are the stop and start times of each pass. For each of the five gravity models, the two arcs of Doppler data were used to determine an orbit. The numerical integration was performed with an Adams-Cowell twelfth-order integrator having a two-minute time step. The starting times for the differential correction on both data arcs are given in Figure 1.

The five gravity fields which were used in the study were the tri-axial, R2, L1 and R6 fields. Field 15, which was derived by Felsentreger, Murphy, Ryan and Salter, was also tried (reference 1). The coefficients of the five lunar potential

COMPARISON OF LUNAR GRAVITY FIELDS USING GSFC RANGE-RATE DATA FROM AIMP-E

1. INTRODUCTION

The orbit of AIMP-E (launched on July 19, 1967) is markedly different from that of the other lunar satellites in the Apollo and Lunar Orbiter series. The orbit has a minimum height above the lunar surface of 790 kilometers with an eccentricity of 0.5739. Since AIMP-E has such a high orbit, lunar mass concentration effects are negligible and only the major terms in the lunar gravitational potential and the perturbations due to the sun and the earth effect the AIMP-E orbit.

The STADAN network is still tracking AIMP-E in lunar orbit using the VHF GRARR system. Some studies have been made to evaluate the lunar satellite tracking capability of the GRARR VHF system. Since future lunar orbiting satellites, such as Radio Astronomy Explorer (RAE-B), will also use VHF range-rate data, the following analysis also has a direct application.

There are two practical methods of estimating the lunar satellite tracking capability of Stadan VHF GRARR range-rate data. One method is to determine the magnitude of the Doppler frequency residuals in a converged solution for the AIMP-E orbit. Another approach is to determine the accuracy with which one can project or predict an orbit based on VHF Doppler observations. In this report trajectory evaluations were performed for each of five lunar potential models. The magnitudes of the position differences obtained in the various trajectory intercomparisons give an indication of the prediction capability of each gravity model.

2. AIMP-E ORBITAL SOLUTIONS

To study the orbit of AIMP-E, two consecutive three-day data arcs of VHF two-way Doppler data were obtained. The data were obtained by tracking stations operating at an uplink frequency of 148.26 MHz and a downlink frequency of 12/13 the uplink frequency. The summary of contents for each data arc is listed in Table 1. Included in this table are the stop and start times of each pass. For each of the five gravity models, the two arcs of Doppler data were used to determine an orbit. The numerical integration was performed with an Adams-Cowell twelfth-order integrator having a two-minute time step. The starting times for the differential correction on both data arcs are given in Figure 1.

The five gravity fields which were used in the study were the tri-axial, R2, L1 and R6 fields. Field 15, which was derived by Felsentreger, Murphy, Ryan and Salter, was also tried (reference 1). The coefficients of the five lunar potential

models are listed in Table 2. The program input constants are listed in Table 3. The geocentric coordinates of the VHF transmitting stations are given in Table 4.

3. DOPPLER RESIDUAL MAGNITUDES

The first gravity field used with AIMP-E Doppler data was the L1 field. After four iterations of the LUNGFISH (Lunar Gravity Field in Spherical Harmonics) computer program, a converaged solution for the orbit was obtained using the second data stretch (August 23 to 26, 1968). The Doppler frequency residuals are plotted on Figures 2-5. The pass for station 52 (i.e., Carnarvon) has a duration of four minutes. The plotted residuals are bounded by an envelope. The envelope results because the range-rate data is recorded at a sampling frequency of one measurement per second which is shorter than the spin period of 2.41 seconds (reference 3). The envelope period of about 48 seconds contains an integral number of 20 spin periods.

One method of gauging the quality of STADAN VHF Doppler data would be to compare the sum of squares and the sigma of the Doppler frequency residuals for each converged run. These two quantities are tabulated for each gravity model using both data arcs in Table 5. The values of sigma run from .4 to .5 Hz. For STADAN VHF data, one Hz of two-way Doppler frequency is equivalent to 1.1136 meters/sec. The residuals, therefore, correspond to 40 to 50 cm/sec. In this study it was found that these residual magnitudes were of little significance in evaluating VHF range rate data. If all modeling errors are eliminated (ionosphere correction, satellite spin modulation and spin bias) the VHF GRARR system can achieve a resolution of 6 cm/sec using a sampling rate of 1 second (reference 5). The high noise level of 40 to 50 cm/sec obtained in the LUNGFISH runs is the result of AIMP spin cyclic modulation (in contrast to spin bias) effects. Spin modulation produces range-rate residuals that contain periodicities related to the spin of the satellite and the data sampling rate. The periodicities are caused by variations in the phase pattern of the antenna. In addition antenna rotation introduces a fixed bias in range rate measurement, (reference 3). The observation data was unsmoothed and data smoothing was left to the LUNGFISH orbit determination program. This procedure does not smooth spin bias. Thus the residuals appear somewhat high but this should not detract from the orbit computation accuracy. The magnitude of the residuals can be greatly reduced by fitting polynomials to the unsmoothed data prior to orbit computation. However, such data compression techniques were not employed during this analysis in order to preclude introducing any bias due to smoothing.

4. ORBIT COMPARISONS

Another method of evaluating STADAN VHF GRARR data is to determine how accurately orbits can be predicted using this data. Such a study also permits

comparison of the predicting capability for the various lunar gravity models. For each gravity field, a propagated orbit (August 20 to 26) and a solution orbit (August 23 to 26) were obtained by differential corrections using the first and second data arcs respectively. The converged solution for the starting vector for each run is given in selenographic Kepler elements in Table 6.

It is obvious that the starting vectors are almost identical for the tri-axial, R2 and L1 fields. The starting vectors for the R6 and Field 15 potential models are slightly different from those predicted by the previous fields. Since the starting vectors are so similar, one can expect the deviation of the solution orbit from the predicted orbit to be fairly similar for the five gravity fields. These results were expected because AIMP-E is in a high lunar orbit and the fields contain similar low-order and low-degree coefficients.

The deviation of the solution orbit from the propagated orbit was transformed from selenocentric coordinates to radial, along-track and cross-track position differences. These trajectory differences are plotted on Figures 6-11. The graphs of the trajectory differences using each field exhibit a variety of forms. Most of the graphs have curves with a period equal to the orbital period of AIMP-E. Some curves appear to be periodic in nature, while others exhibit combinations of secular and periodic effects. For example, the position differences for the L1 field and Field 15 vary in the following ways: The L1 field has radial position differences that range from - 1.1 to + 1.3 km per orbital period at August 22, 19 hours GMT, 1968. Five orbits later, the radial position differences range from a minimum of -3 km to a maximum of +3.3 km per orbital period. The along-track error differences range from 2.1 to 4.0 km per orbital period at August 22, 19 hours GMT while five orbits later the maximum and minimum are 9.3 and 3.8 km respectively. The cross-track position differences appear to be periodic with maxima and minima of +12 and -41 km respectively. (The position differences of the R2 field are almost identical to those of the L1 field). In comparison, Field 15 had a radial position difference curve which appears to be periodic with an amplitude ranging from -1.1 to 1.5 km. The along-track position differences vary slowly from .4 to 6.0 km per orbital period at August 22, 19 hours GMT, 1968 and six orbits later vary from -.9 to 4.9 km per period. The cross-track differences appear to be periodic ranging from -44 to +14 km. Field 15 is seen to be superior in that over the three-day time interval, the radial and along-track position differences for Field 15 are almost periodic maintaining about the same maximum amplitude and form. For the other fields, the maximum amplitude of the radial and the along-track trajectory differences increase with each orbital revolution of AIMP-E. The largest position difference component for each of the five-fields is the cross-track component probably because range-rate supplies little information on the orientation of the orbital plane.

Field 15 does minimize the differences better than the other fields. However another factor in addition to gravity models seems to be very important in this study of trajectory differences. Since AIMP-E has a highly eccentric orbit, it spends a great deal of time near apolune. This causes certain problems in obtaining uniformly distributed data over the orbit. Due to satellite tracking schedules followed by the stations very few passes of data for AIMP-E last longer than five minutes. Since the orbital period is 11.52 hours, these passes form very short arcs. In the data processed for this report apolune was located at selenographic longitude 80°E on August 19, 19 hours and at longitude 45°E on August 22, 16 hours. All of the data in each arc was taken when the satellite was 55 degrees on either side of apolune. If data were taken over the entire visible portion on the AIMP-E orbit rather than over just one quadrant, then the magnitude of the trajectory differences would be considerably reduced. This would require knowledge of the apolune and perilune times of AIMP-E at the tracking stations.

5. SUMMARY

This work accomplished two objectives. It served as an evaluation of STADAN VHF GRARR tracking performance in absence of modeling spacecraft spin and ionospheric range-rate bias. If these quantities were modeled, the magnitude of the residuals of the original unsmoothed data would be greatly reduced. It is expected that the noise in the range-rate residuals would then be reduced from 40 to 50 cm/sec and would approach the resolution of 6cm/sec (if a 1 second sampling rate were used) which is expected of the VHF GRARR system. These reduced residuals would be a measure of the accuracy that can be achieved. The second objective of the study was to indicate to what degree various lunar gravity fields influence orbit computation based on unsmoothed VHF GRARR data. The results of this study show that Field 15 (reference 1) minimizes the magnitude of the trajectory differences for AIMP-E better than the other four lunar gravity models using the August 20 to 26 (1968) AIMP-E range-rate data stretch. More uniform distribution of data over the orbit should further help to minimize the trajectory differences.

6. ACKNOWLEDGMENTS

The author is grateful to James Murphy, Ted Felsentreger and Paul Schmid for their careful reviews of this work and for their many helpful suggestions. Paul Schmid provided us with the appropriately formatted STADAN data and he advised us regarding its use. The author also wishes to thank Arthur Fuchs who provided initial orbital elements on AIMP-E.

7. REFERENCES

1. Felsentreger, T. L., Murphy, J. P., Ryan, J. W., and Salter, L. M. "Lunar Gravity Fields Determined from Apollo 8 Tracking Data." GSFC X-552-69-317, (July, 1969).

2. Fuchs, A. J. "AIMP-E Real-Time Orbit Determination Support Summary." GSFC X-832-67-571, (November, 1967).

3. Marini, J. W., and Murray, C. W. "Effect of Satellite Spin on Explorer 33 and 35 Doppler Tracking Data." GSFC X-551-69-52, (February, 1969).

4. Schmid, P. E. "The Conversion of Fundamental Tracking Data to Metric Form." GSFC X-551-69-3 (January, 1969).

5. General Dynamics. "Goddard Range and Range Rate System Design Evaluation Report." No. R-67-042, (December 13, 1967).

8. ABBREVIATIONS

AIMP-E	Anchored Interplanetary Monitoring Platform-E (Explorer 35)
d	Day
GMT	Greenwich Mean Time
GRARR	Goddard Range and Range Rate System
hr or h	Hour
Hz	Hertz, a cycle per second, unit of frequency
km	Kilometer
LUNGFISH	A computer program that was written by Computer Usage Co. for Langely S.F.C. to determine the gravity field of the moon from Lunar Orbiter range and range-rate data. At the program's inception it handled only Deep Space Network data. At present it can also process MSFN and STADAN data. The mnemonics stand for Lunar Gravity Field in Spherical Harmonics.

min or m	Minute
MHz	Megahertz
R_c	Radius of the moon
RAE	Radio Astronomy Explorer (Lunar Mission)
sec or s	Second
STADAN	Space Tracking and Data Acquisition Network
μ_c, $\mu_\oplus$, $\mu_\odot$	Gravitational constants of the moon, earth and sun
VHF	Very High Frequency — Frequency range of 30 to 300 MHz

Table 1

Summary of AIMP-E Tracking Data (Two Arcs)

DATA ARC 1

Pass No.	No. Obs.	Start-Time		End-Time		Station
		Day	H/M/S	Day	H/M/S	
1	274	233	024802	233	025301	28
2	218	233	142005	233	142451	27
3	291	233	160802	233	161304	26
4	375	233	180621	233	181119	28
5	292	234	013327	234	013822	52
6	236	234	033219	234	033722	52
7	285	234	052211	234	052657	52
8	238	234	150338	234	150832	26
9	295	234	170119	234	170617	28
10	187	235	003103	235	003618	52
11	31	235	024415	235	024445	52
12	319	235	120134	235	120704	26
13	268	235	140111	235	140542	27
14	284	235	160122	235	160617	28
15	244	235	180948	235	181359	27
16	300	235	233117	235	233616	28

Data Arc 1 contains 16 passes and 4137 usable observations scattered over six 11.52 hour orbits of AIMP-E

Table 1 (Continued)

DATA ARC 2

Pass No.	No. Obs.	Start-Time		End-Time		Station
		Day	H/M/S	Day	H/M/S	
17	48	236	014747	236	014958	52
18	308	236	033451	236	033958	52
19	171	236	054155	236	054509	52
20	271	236	130058	236	130544	27
21	303	236	150514	236	151200	26
22	184	236	171657	236	172000	28
23	299	236	223136	236	223634	28
24	375	237	003113	237	003612	28
25	296	237	024239	237	024734	52
26	287	237	043803	237	044249	52
27	307	237	155113	237	155603	27
28	268	237	212147	237	212642	28
29	243	237	231755	237	232458	28
30	300	238	012807	238	013306	52
31	235	238	032027	238	032425	52
32	276	238	145454	238	145953	27
33	279	238	201629	238	202127	27
34	287	238	221623	238	222121	28
35	307	239	021807	239	022313	52

Data Arc 2 contains 19 passes and 5044 usable observations scattered over six 11.52 hour orbits of AIMP-E

Table 2

Lunar Gravity Models

Cor S	N	M	Tri-Axial Field	R2 Field	L1 Field	R6 Field	Field 15
C	2	0	-207.1867	-207.108	-207.108	-210.	-198.7651
C	3	0		21.0	21.0	16.	- 75.66981
C	4	0					
C	2	1					
C	3	1		34.	34.	32.	53.86133
C	4	1					
C	2	2	20.23974	20.716	20.716	21.	49.0906
C	3	2					
C	4	2					
C	3	3			2.583		
C	4	3					
C	4	4					.1139595
S	2	1					
S	3	1				10.	- 29.08456
S	4	1					
S	2	2					- 14.05312
S	3	2					
S	4	2					
S	3	3					
S	4	3					
S	4	4					- .2008823

* Multiple all coefficients by 10^{-6}

Table 3

List of Constants

$\mu_{\mathbb{C}}$	= 4,902.778 km ^{3}/sec ^{2}
$\mu_{\oplus}$	= 398,604.6 km ^{3}/sec ^{2}
$\mu_{\odot}$	= .13271482 × 10^{12} km ^{3}/sec ^{2}
$R_{\mathbb{C}}$	= 1738.09 km
c	= 299,792.5 km/sec

Table 4

Geocentric Station Coordinates

Transmitting Station NR	R Radius (km.)	PHI Latitude 0	1	11	LAMBDA Longitude 0	1	11
22 TAN	0.6377320D 04	-18	54	06.22	47	18	12.56
26 ROS	0.6371978D 04	35	00	50.13	277	07	26.89
27 SAN	0.6372503D 04	-32	58	30.90	289	19	59.78
28 FRB	0.6361008D 04	64	49	25.96	212	29	21.11
52 CRO	0.6374450D 04	-24	45	30.85	113	42	55.06

Table 5

Sigma for Doppler Frequency Residuals

Case No.	Epoch of Converged Starting Vector	Time Span of Data Arc	Number of Observations	Lunar Gravity Model	Sum of Squares Hz^2	Sigma Hz
1	$68^y 232^d 19^h 26^m$	$233^d 2^h$—$235^d 23^h$	4137	TRI-Ax	822.1897	.44580
2	$68^y 232^d 19^h 26^m$	$233^d 2^h$—$235^d 23^h$	4137	R2	822.1359	.44578
3	$68^y 232^d 19^h 26^m$	$233^d 2^h$—$235^d 23^h$	4137	L1	821.9883	.44574
4	$68^y 232^d 19^h 26^m$	$233^d 2^h$—$235^d 23^h$	4137	FIELD-15	824.1382	.44633
5	$68^y 232^d 19^h 26^m$	$233^d 2^h$—$235^d 23^h$	4137	R6	822.2421	.44581
6	$68^y 235^d 16^h 36^m$	$236^d 2^h$—$239^d 2^h$	5044	TRI-Ax	1275.623	.50289
7	$68^y 235^d 16^h 36^m$	$236^d 2^h$—$239^d 2^h$	5044	R2	1274.573	.50268
8	$68^y 235^d 16^h 36^m$	$236^d 2^h$—$239^d 2^h$	5044	L1	1274.823	.50273
9	$68^y 235^d 16^h 36^m$	$236^d 2^h$—$239^d 2^h$	5044	FIELD-15	1270.209	.50182
10	$68^y 235^d 16^h 36^m$	$236^d 2^h$—$239^d 2^h$	5044	R6	1275.877	.50299

*One Hz of two-way Doppler frequency is equivalent to 1.1136 meters/second.

Table 6

Selenographic Keplerian Elements at Epoch

Case No.	Field	Day	a (kilometers)	e	ι (degrees)	Ω (degrees)	α (degrees)	M (degrees)
1	TRI-Ax	232	5977.4034	.585694	166.230	-63.8322	33.3977	-174.065
2	R2	232	5977.4099	.585780	166.234	-63.4084	33.8183	-174.069
3	L1	232	5977.4097	.585781	166.222	-63.3932	33.8339	-174.069
4	F15	232	5977.3367	.585906	166.266	-63.2606	33.9743	-174.089
5	R6	232	5977.4308	.585762	166.228	-63.3759	33.8448	-174.061
6	TRI-Ax	235	5980.6214	.573895	166.172	-99.8659	34.4783	-173.041
7	R2	235	5980.6744	.573916	166.233	-99.4920	34.8409	-173.016
8	L1	235	5980.6748	.573914	166.233	-99.4791	34.8533	-173.015
9	F15	235	5980.6847	.574040	166.287	-99.2022	35.1318	-173.011
10	R6	235	5980.6832	.573896	166.238	-99.4464	34.8828	-173.011

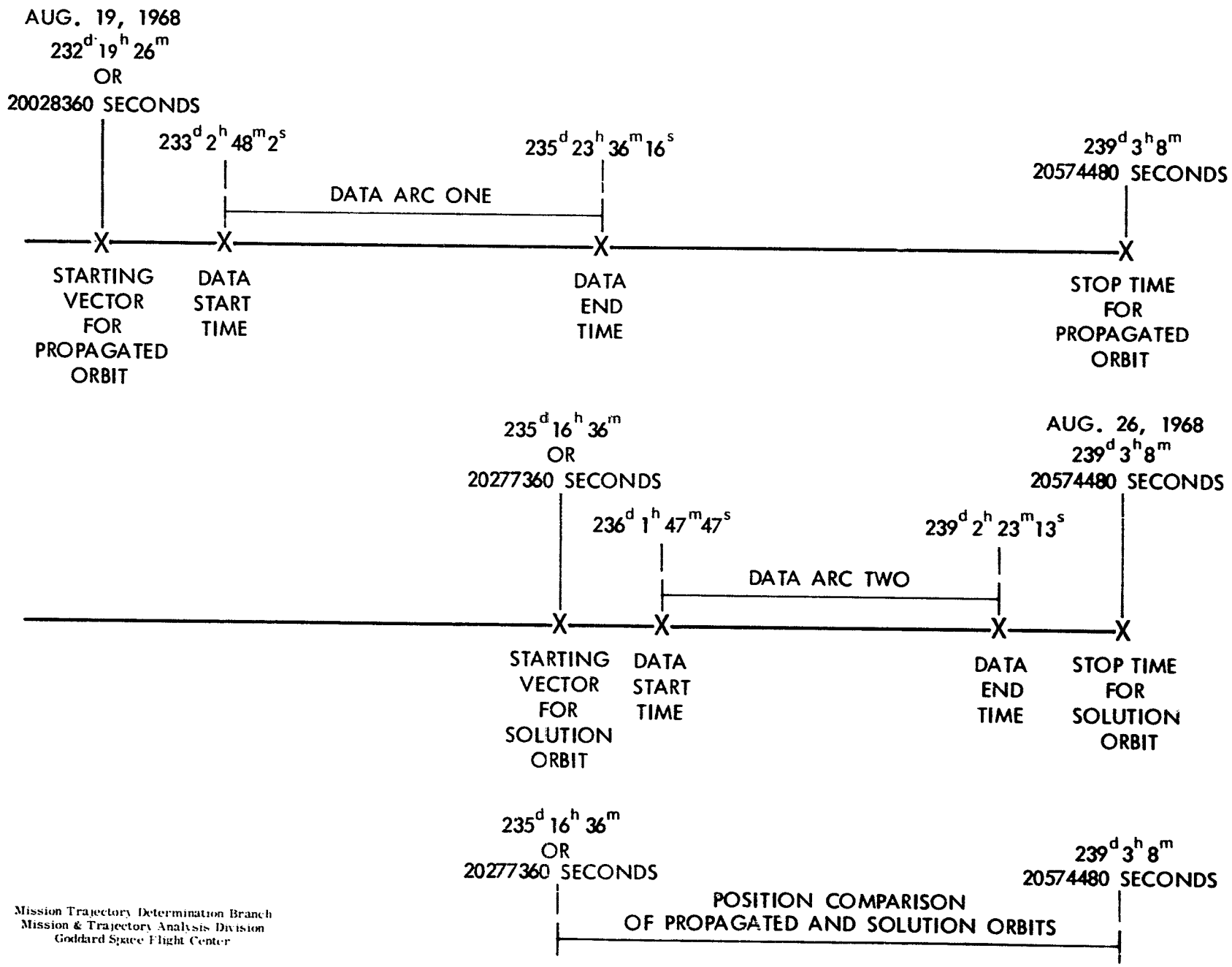

Mission Trajectory Determination Branch
Mission & Trajectory Analysis Division
Goddard Space Flight Center

Figure 1. Greenwich mean times associated with each of the two data arcs and with the propagated and solution orbit.

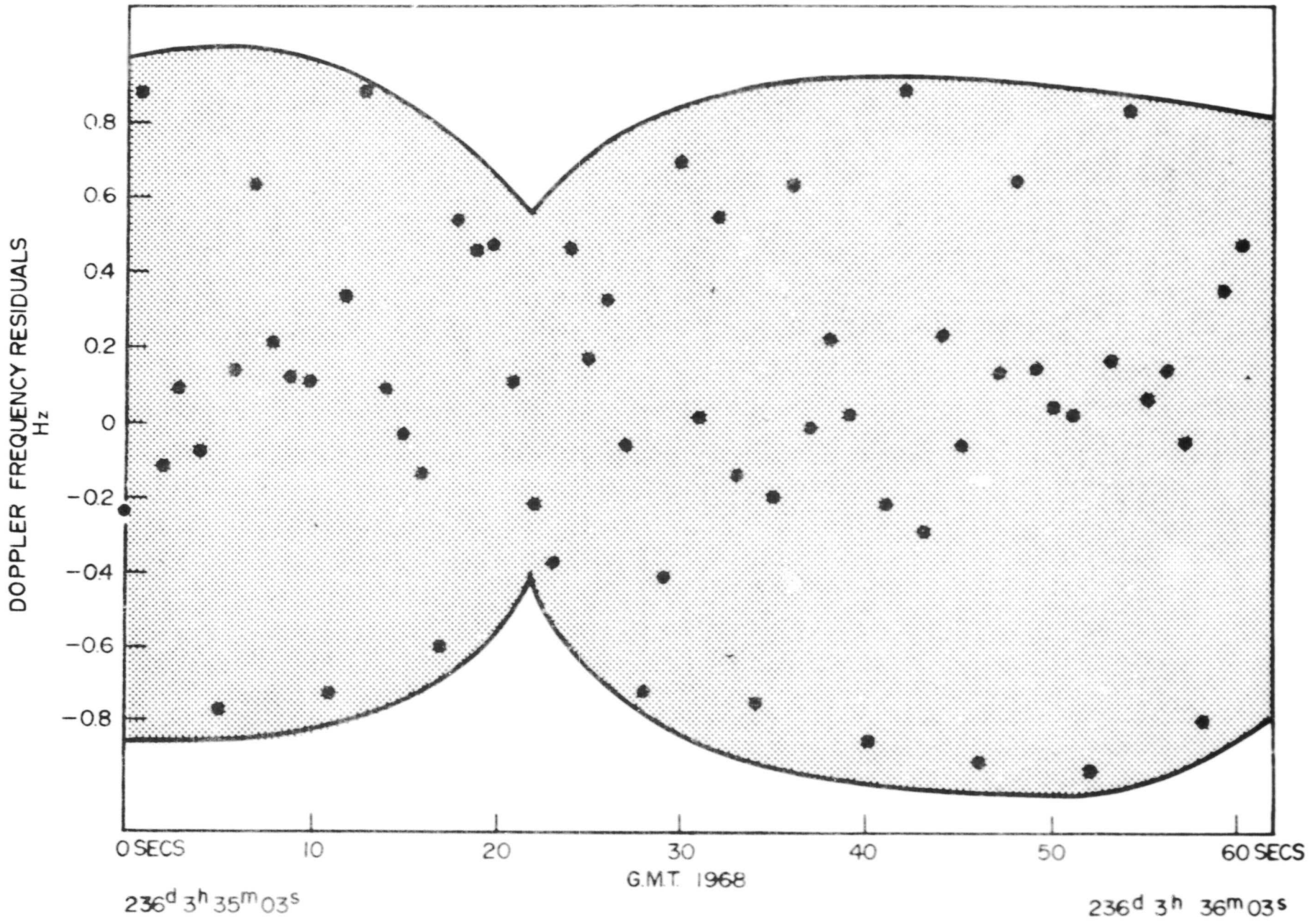

*One Hz of two-way Doppler frequency is equivalent to 1.1136 meters/sec.

Figure 2. Doppler residual plot for the L1 field with data from station 52.

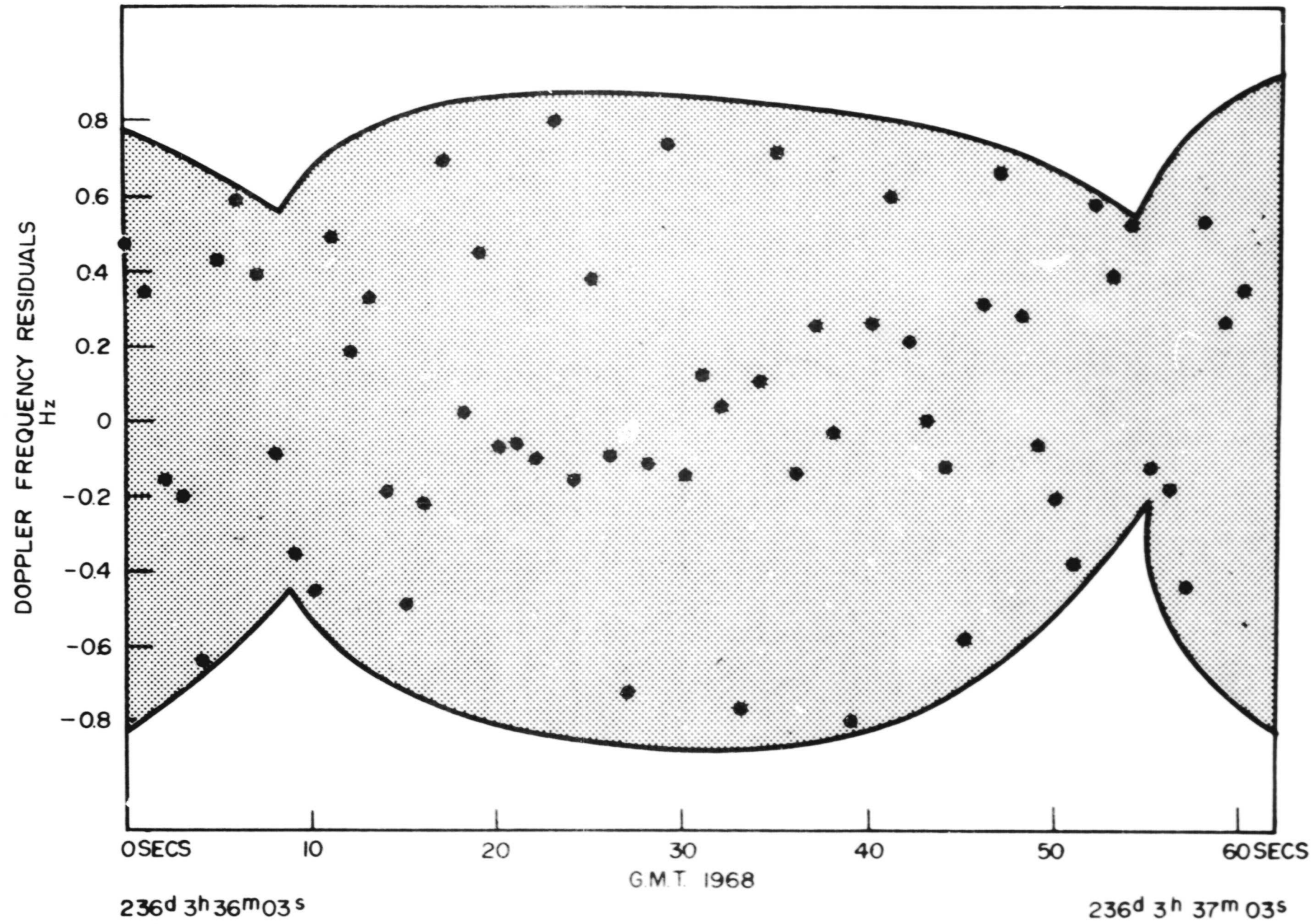

Mission Trajectory Determination Branch
Mission & Trajectory Analysis Division
Goddard Space Flight Center

Figure 3. Doppler residual plot for the L1 field with data from station 52.

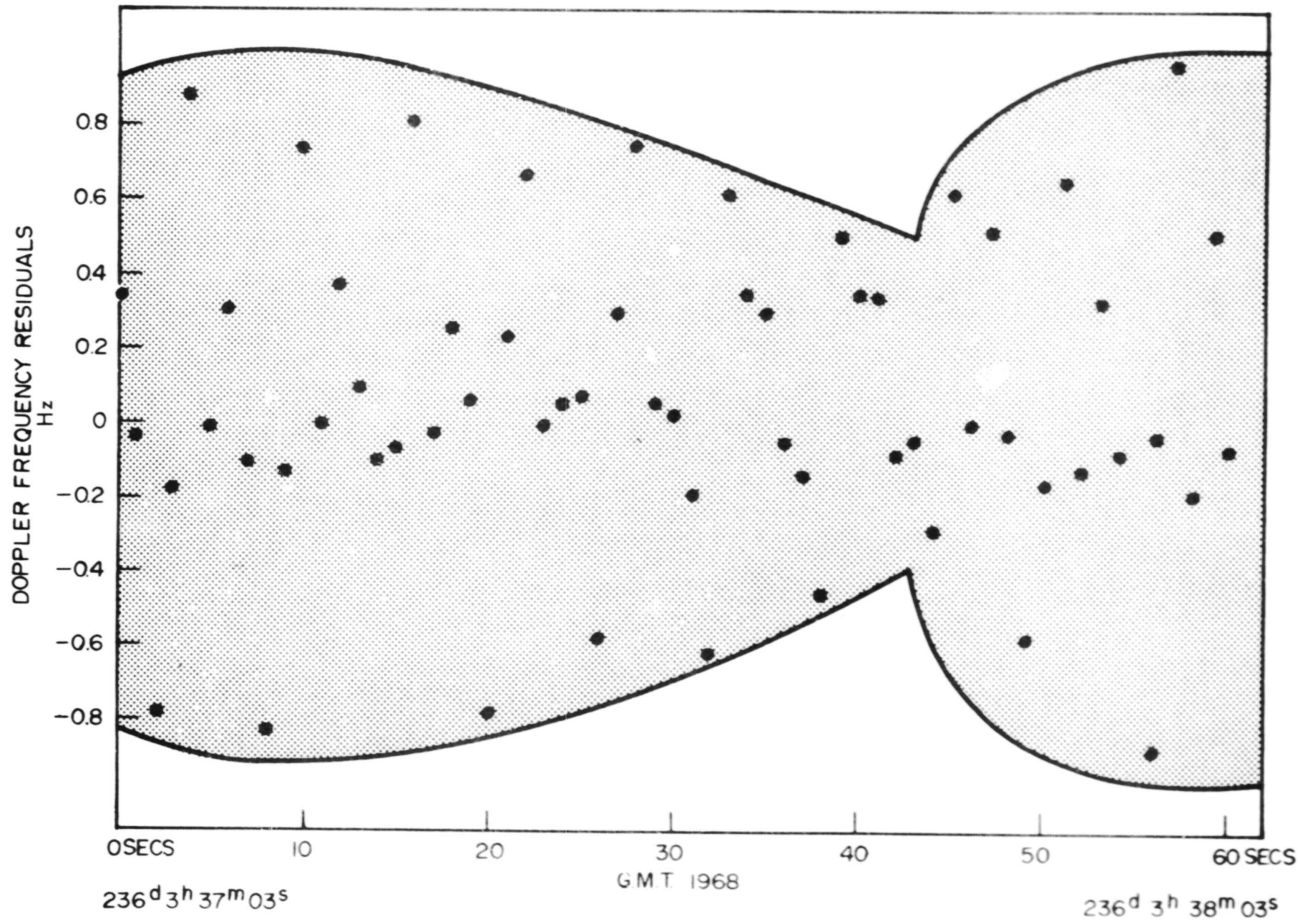

Mission Trajectory Determination Branch
Mission & Trajectory Analysis Division
Goddard Space Flight Center

Figure 4. Doppler residual plot for the L1 field with data from station 52.

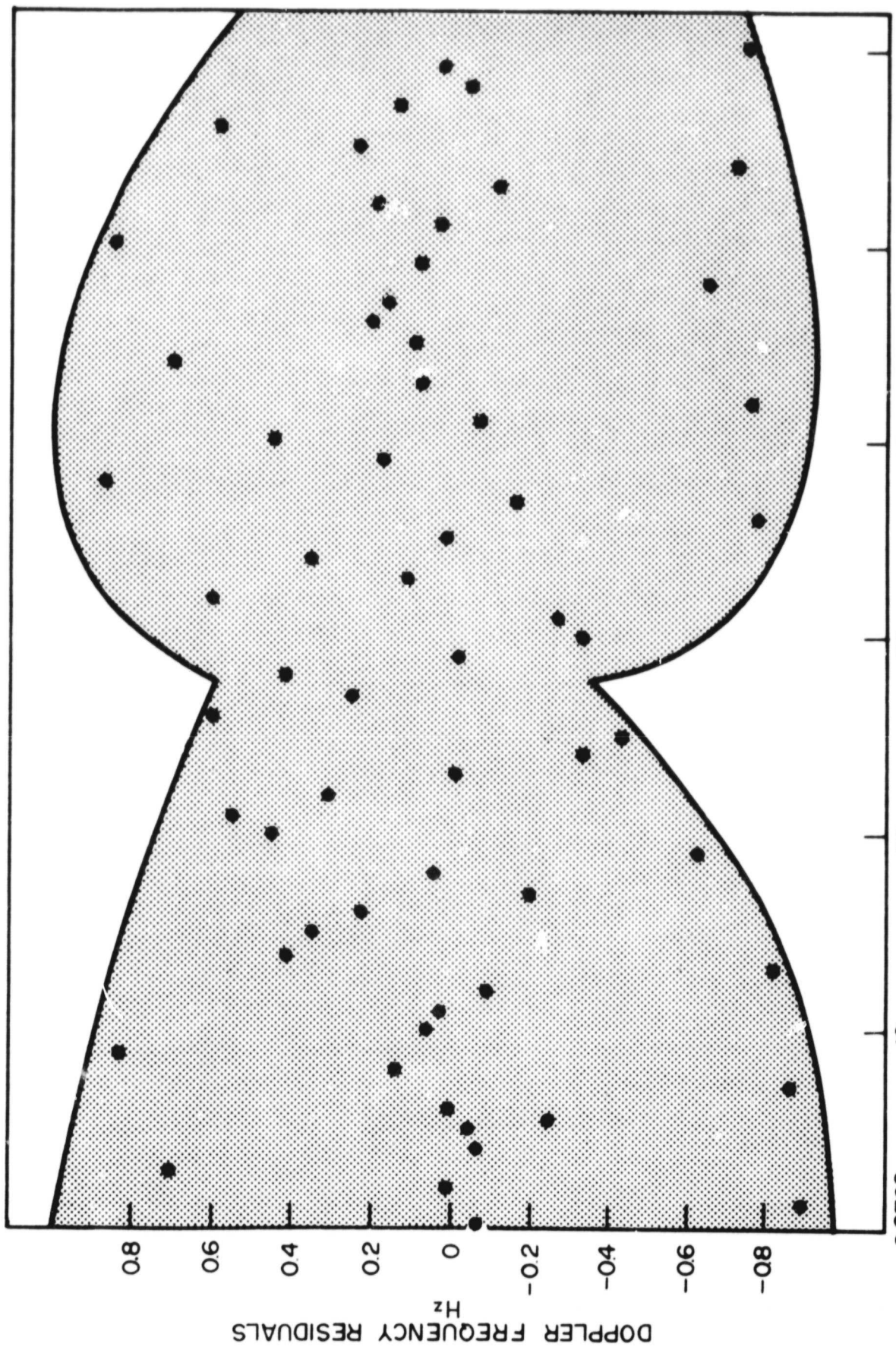

Figure 5. Doppler residual plot for the LI field with data from station 52.

Mission Trajectory Determination Branch
Mission & Trajectory Analysis Division
Goddard Space Flight Center

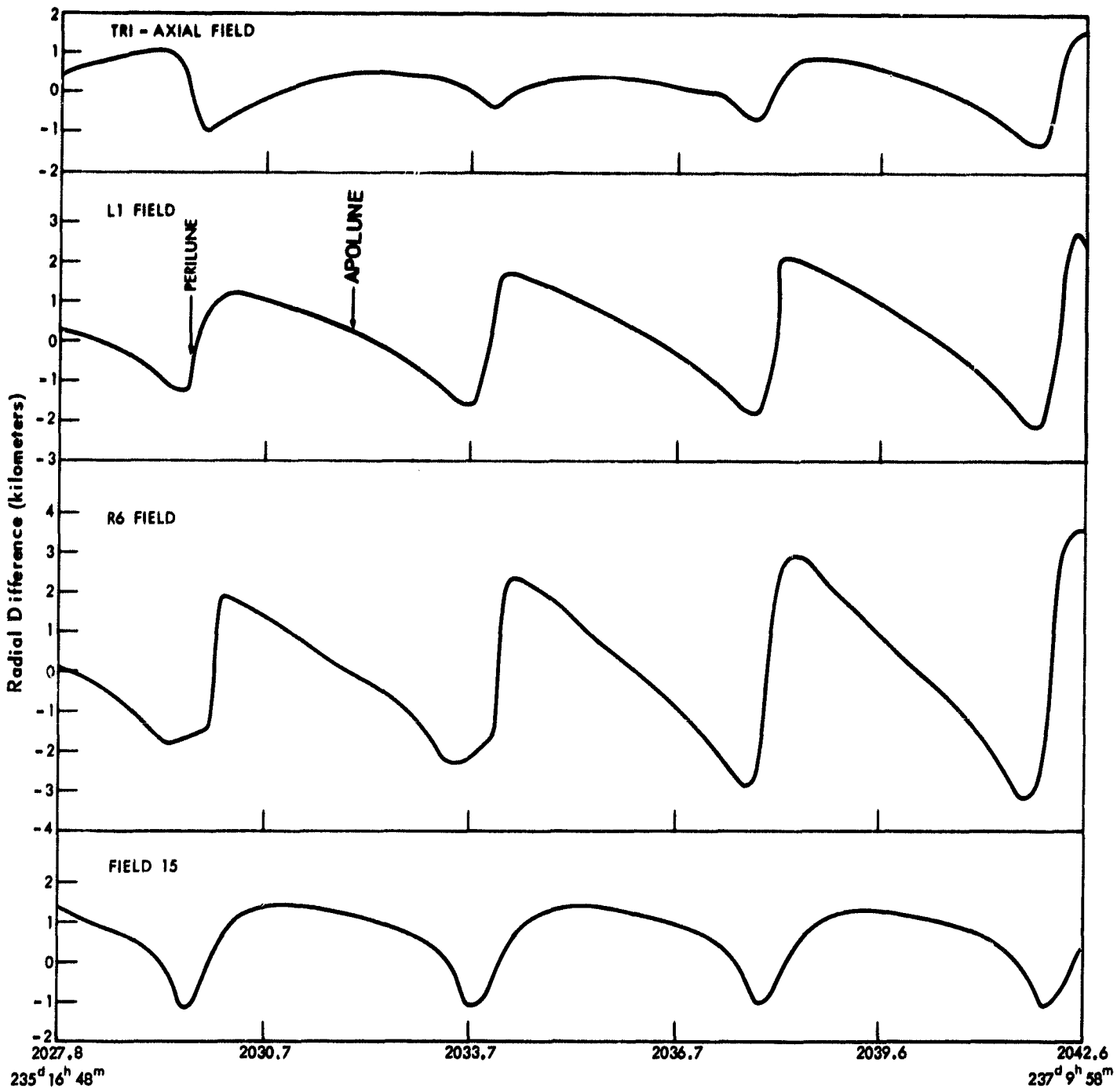

Mission Trajectory Determination Branch
Mission & Trajectory Analysis Division
Goddard Space Flight Center

Figure 6. Radial difference as a function of time for four lunar gravity fields.

***Radial position differences are measured along the selenocentric radius vector.**

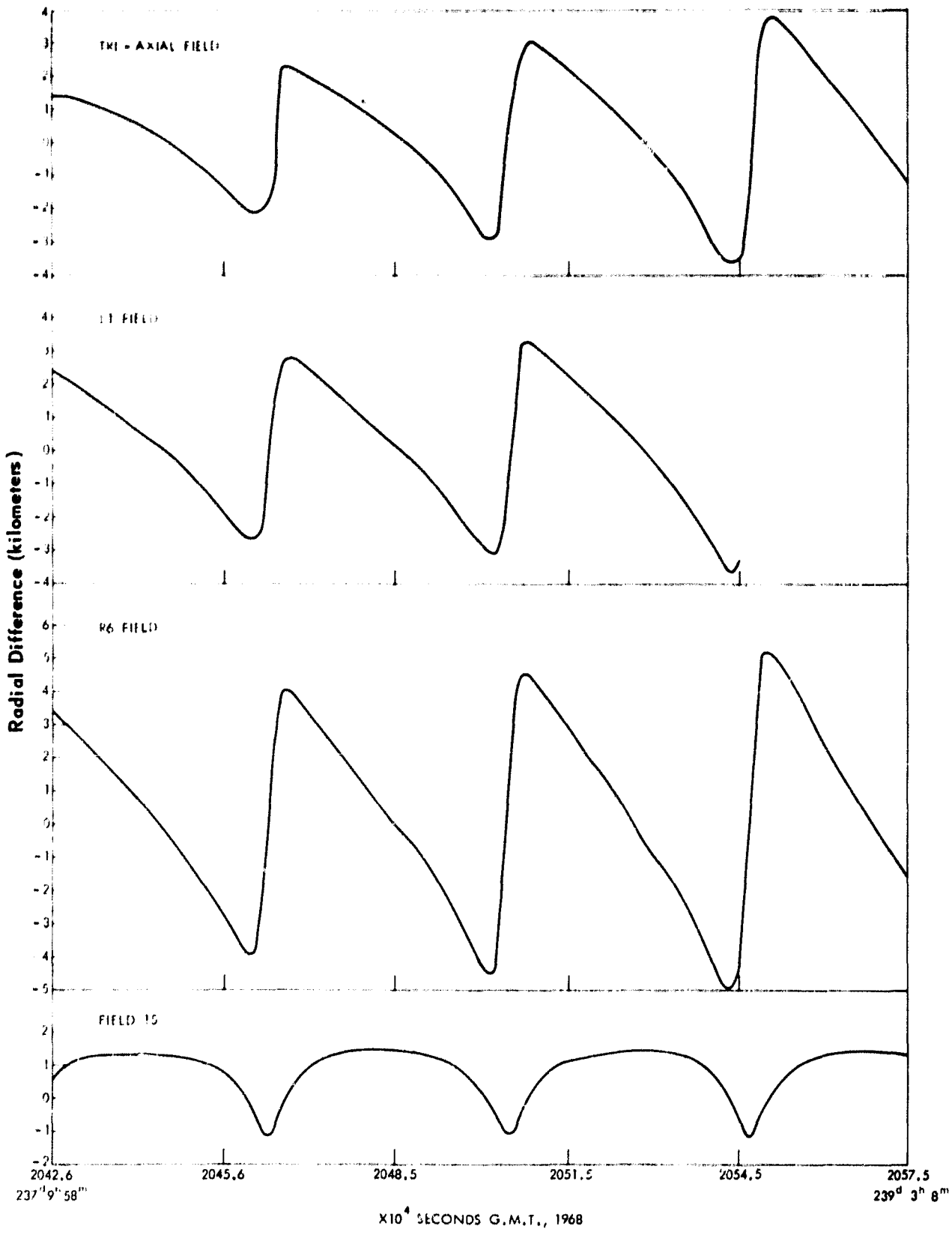

Figure 7. Radial difference as a function of time for four gravity fields.

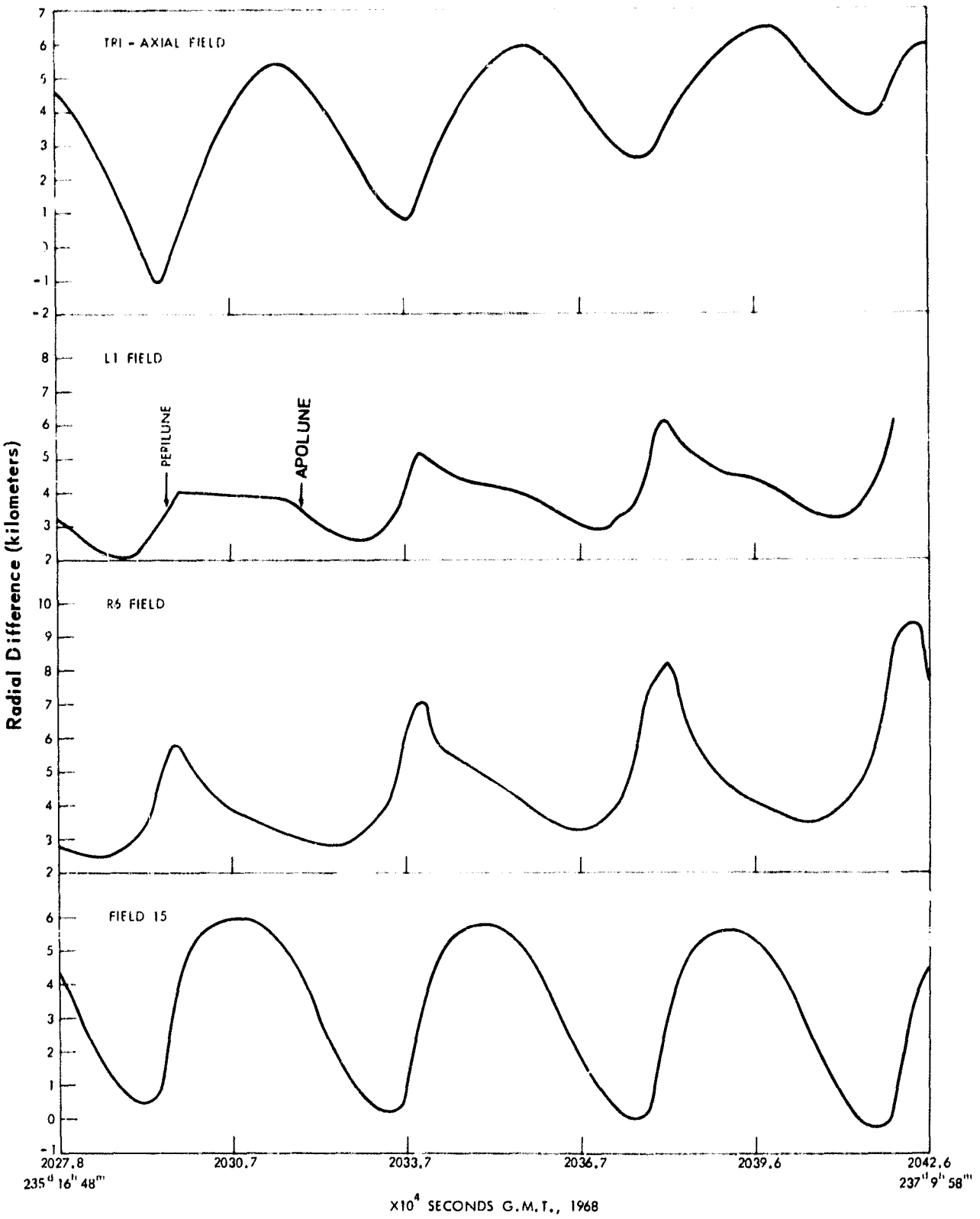

Mission Trajectory Determination Branch
Mission and Trajectory Analysis Division
Goddard Space Flight Center

Figure 8. Along-track difference as a function of time for four gravity fields.

* Along-track differences are measured in the orbital Plane.

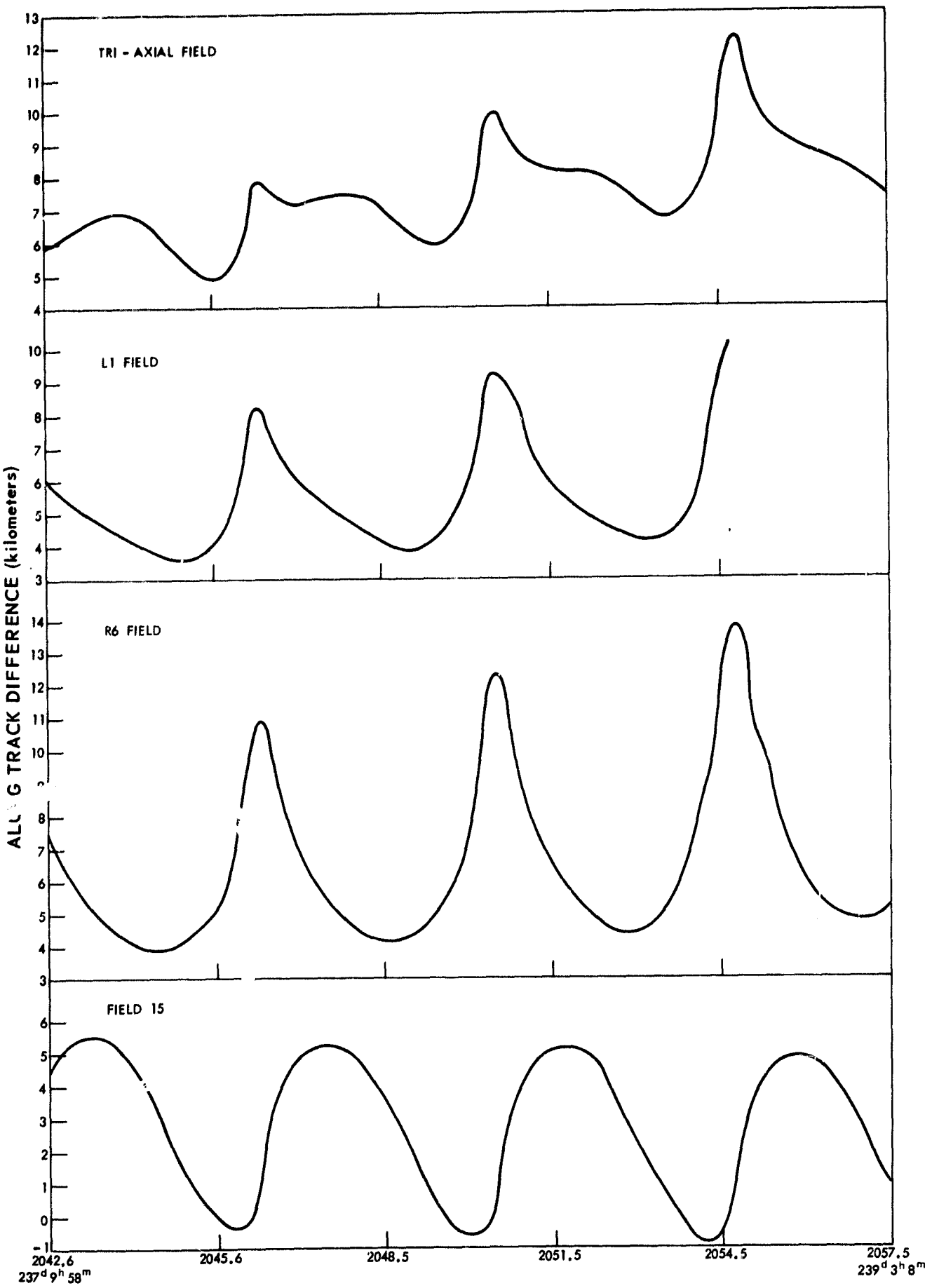

Figure 9. Along-track difference as a function of time for four gravity fields.

Mission Trajectory Determination Branch
Mission and Trajectory Analysis Division
Goddard Space Flight Center

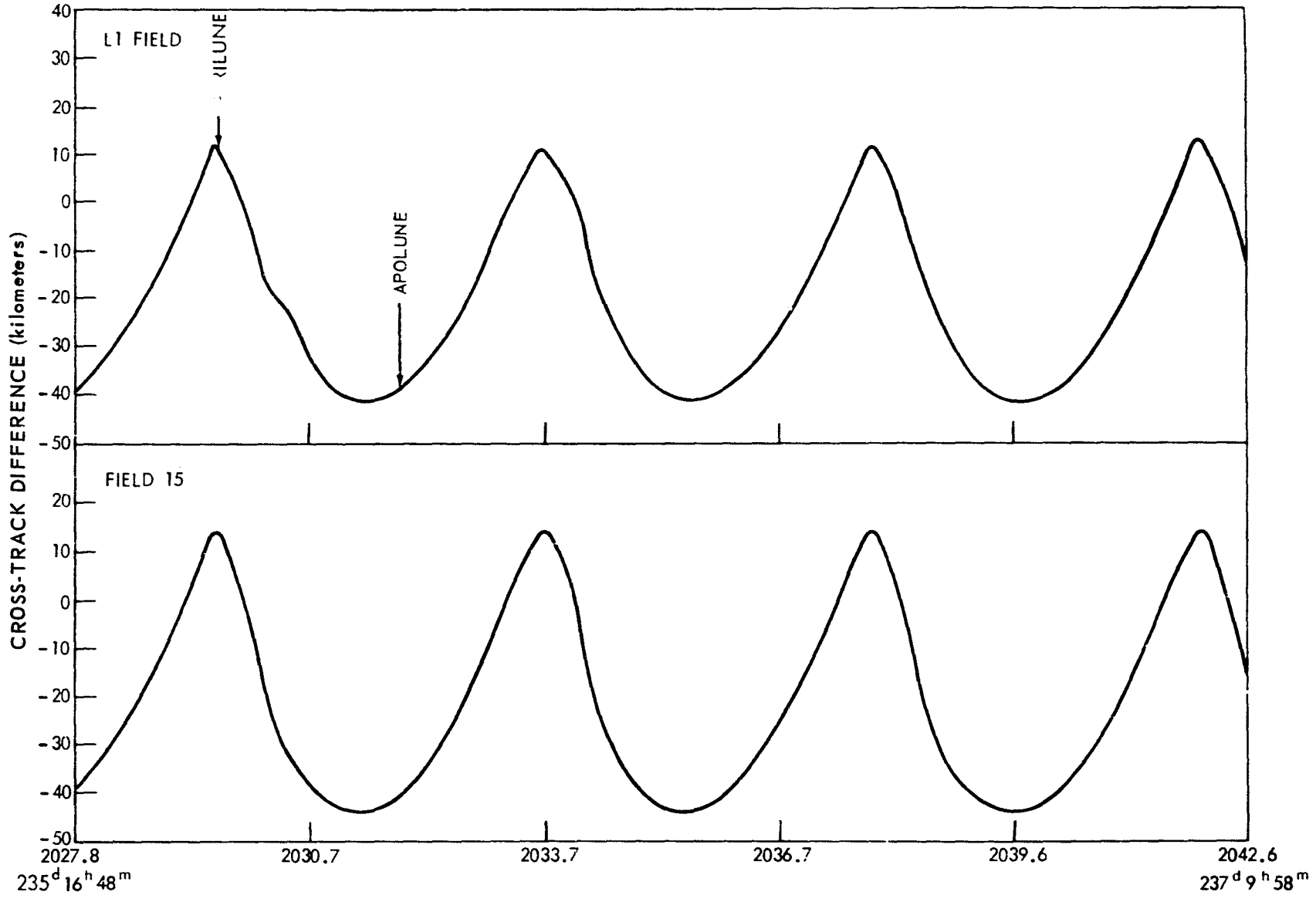

Figure 10. Cross-track difference as a function of time for four gravity models.

* Cross-track differences are measured perpendicular to the orbital plane.

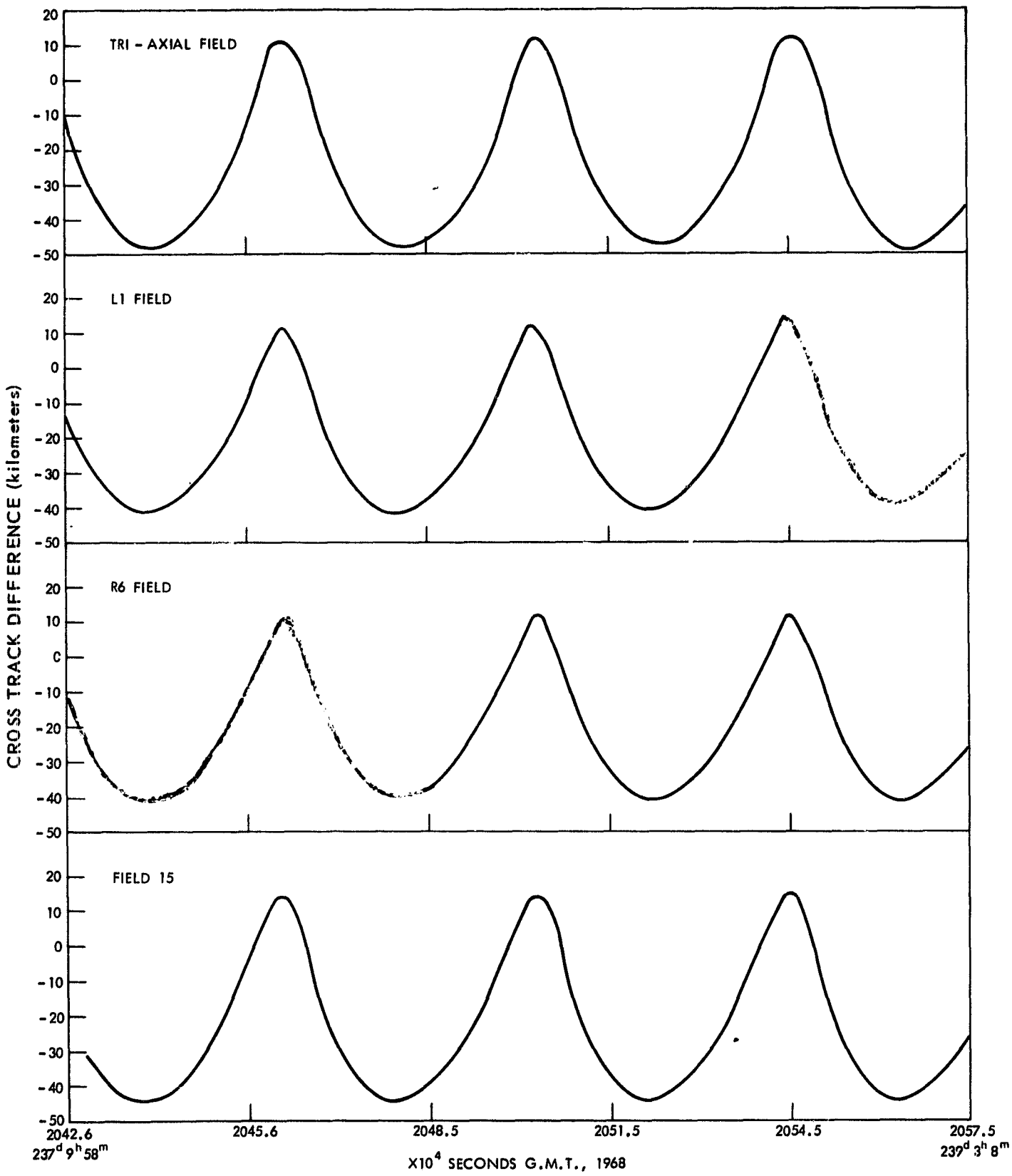

Mission Trajectory Determination Branch
Mission and Trajectory Analysis Division
Goddard Space Flight Center

Figure 11. Cross-track difference as a function of time for four gravity models.